

OPTICAL BIOSENSORS PROSPECTIVE BASED ON BRAGG GRATING POLYMER WAVEGUIDE

Mohd Hazimin Mohd Salleh^{a*}, Mohd Haziq M.S^b, Muhammad Salihi Abd Hadi^c

^aDepartment of Physics, Kulliyah of Science, International Islamic University Malaysia (IIUM), 25200 Kuantan, Pahang, Malaysia

^bDepartment of Computer Science, Kulliyah of Information and Communication Technology, International Islamic University Malaysia (IIUM), Gombak, 50728 Kuala Lumpur, Malaysia

^cDepartment of Computational and Theoretical Science, Kulliyah of Science, International Islamic University Malaysia (IIUM), 25200 Kuantan, Pahang, Malaysia

Article history

Received

15 August 2015

Received in revised form

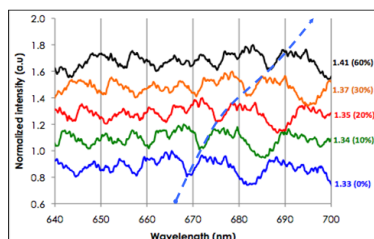
15 November 2015

Accepted

30 December 2015

*Corresponding author
mhazimin@iium.edu.my

Graphical abstract



Abstract

In this work, we demonstrate the potential of Bragg grating polymer waveguide as an optical biosensor. Visible wavelength region at 650 nm is used as a centre wavelength because it is commonly used in biological and chemical sensing for both label and label-free sensing. The Bragg polymer waveguide structure is simulated using RSoft optical design and analysis software. The results show that there is a transmission drop with a 3 dB bandwidth of 661.0 nm when the surrounding refractive index is 1.33. The specific wavelength (transmission drop) is shifted to 724.2 nm when we increased the surrounding medium into 1.43 to mimic the bioanalytes solution. Simulation result shows that the wavelength shift was approximately 63.2 nm for every 0.1 increasing of surrounding refractive index. The Bragg grating polymer waveguide was fabricated by using electron beam lithography. Then, the fabricated devices were easily integrated within microfluidic systems in order to validate the wavelength shift. From the experiments, the wavelength shift occurred approximately 20.3 nm over 0.1 increment of refractive index. The discrepancies were likely due to the accumulation of sucrose solution on top and sidewall of the sensing area, the insertion loss between input and output coupling of the waveguide interface that induced the noise to signal ratio. Where we know that, is impossible to happen in simulation. Thus both simulation and experimental results strongly indicate that Bragg grating polymer waveguide structure at visible wavelength region have a potential for label or label-free optical biosensing applications.

Keywords: Optical biosensor, Bragg grating, simulation, label-free sensing, polymer waveguide

Abstrak

Dalam kajian ini, kami menunjukkan potensi pandu gelombang berdasarkan parutan Bragg sebagai biopenderia optik. Kawasan panjang gelombang yang boleh dilihat iaitu pada 650 nm telah digunakan sebagai panjang gelombang pusat kerana ia seringkali digunakan dalam kajian yang melibatkan penderiaan biologi dan kimia untuk kedua-dua label dan bebas label. Struktur parutan Bragg yang menggunakan bahan polimer disimulasi menggunakan perisian rekabentuk optik dan analisis RSoft. Hasil kajian menunjukkan bahawa terdapat penurunan kadar keamatan cahaya sebanyak 3 dB pada panjang gelombang 661.0 nm apabila indeks biasan persekitaran penderia adalah

1.33. Pada panjang gelombang yang telah ditentukan, ia didapati bahawa beralih ke posisi 724.2 nm apabila kami meningkatkan indeks biasan medium sekeliling kepada 1.43. Ini adalah bertujuan untuk mensimulasikan interaksi biologi terhadap penderia. Hasil simulasi menunjukkan bahawa peralihan panjang gelombang adalah kira-kira 63.2 nm bagi setiap peningkatan 0.1 indeks biasan persekitaran penderia. Setelah itu, parutan Bragg polimer difabrikasi dengan menggunakan kaedah elektron litografi. Kemudian, peranti yang telah difabrikasi, disepadukan dalam sistem bendalir mikro bagi mengesahkan perubahan yang berlaku. Daripada eksperimen yang telah dijalankan, peralihan panjang gelombang berlaku sebanyak 20.3 nm dengan kenaikan index biasan sebanyak 0.1. Perbezaan nilai peralihan yang diperolehi daripada simulasi dan eksperimen mungkin disebabkan oleh pengumpulan larutan sukrosa di atas dan sisi kawasan sensing, kehilangan keamatan cahaya semasa penjarangan optik antara input dan output penderia. Keadaan ini meningkatkan isyarat kepada hingar semasa eksperimen dijalankan. Di mana kita tahu bahawa, adalah mustahil untuk berlaku dalam kaedah simulasi. Namun demikian, boleh disimpulkan bahawa kedua-dua keputusan simulasi dan eksperimen menunjukkan bahawa gabungan struktur parutan Bragg dengan menggunakan panjang gelombang yang boleh dilihat mempunyai potensi dalam aplikasi penderia biologi/kimia yang menggunakan label atau bebas label.

Kata kunci: Biosensor optik, parutan Bragg, simulasi, penderiaan bebas label, pemandu gelombang polimer

© 2016 Penerbit UTM Press. All rights reserved

1.0 INTRODUCTION

Nowadays, the application of rapid sensing and detection of biological analytes are growing due to the significant environment monitoring [1-2], biological screening [3-4], cell growth [5] and bio/chemical sensors [6, 11-14]. These factors influence the research and development demand of simple, cheap and sensitive functional biomolecular device at very low concentration sample. Meanwhile, the interest in label-free optical detection has increasing since the planar waveguide [9] has a direct light interaction with surrounding analytes, easy integration with microfluidic system and the capability to provide specific interaction.

Basically, a planar waveguide employs an evanescent field on a waveguide surface to interact with analytes of surrounding media. In order to identify a low concentration of active analytes, it is essential to have an extensive detection surface area but at the same time reducing the dimension of the device. Among the planar optical biosensors, Bragg grating waveguide has attracted much interest due to its structure, which offers both the quality of smaller size and further enhancing the sensing surface area. One of the important characteristics of Bragg grating waveguide is the strong evanescent modes can be achieved out of waveguide surface without tapering or etching process, which increase the tendency of strong evanescence field to interact with bio-analytes.

In general, silicon nitride [9], silicon oxide [11-12], silicon-on-insulator (SOI) [13, 23], Hydrex Glass [14-15] are the majority materials for core waveguide of Bragg grating structure. However, silicon-based material is not transparent to the visible light region. For example, silicon Bragg grating waveguide only exists at the communication wavelength region (>1300nm). In

addition, silicon-based material also requires several steps of fabrication process (reactive ion etching (RIE), mask layer deposition etc), which make it complicated to prepare and time consuming compared to polymer-based material. Therefore, silicon-based materials are not suitable prospect for biological sensing that usually utilizing the visible light spectrum [27-29]. As we mentioned earlier, in optical biological sensing, evanescence field on the top surface of waveguide plays very crucial part for light and analytes interaction. For that reason, Bragg grating waveguide has drawn attention for optical biosensors. Various designs and materials have been used to fabricate the structures.

Furthermore, the polymeric based materials offer several advantages over the silica based materials, in terms of their straightforward fabrication process, good surface modification for analytes immobilization and a wide selection of refractive indices. Several polymers have been used in Bragg grating waveguide fabrication such as polymethyl-methacrylate (PMMA) [17-18], polystyrene (PS) [19] and SU8 [27-29]. However, in this paper we only focused on a SU8 polymer (MicroChem Corporation) as a core structure for Bragg grating and straight waveguide. Because SU8 is a negative tone photoresist, an exposed area will be remained on the substrate after the development process.

In this paper, we present a label-free optical detection in biosensing by using Bragg grating polymer waveguide as a sensing structure. The change of refractive index of liquid sample was used to mimic the biomolecular interaction between immobilized sensing area and targets. The optical responses of output waveguide were characterized after refractive index of sensing area was changed deliberately. The visible

wavelength region was utilized as a light source to determine the functionality of the device

2.0 DEVICE FABRICATION

The SU8 polymer Bragg grating waveguides was fabricated on 3.5 μm oxide of wafer by using electron beam lithography (EBL) in James Watt Nanofabrication Centre (JWNC, University of Glasgow). First, the substrates were cleaned ultrasonically by using acetone and Isopropyl alcohol (IPA) for 5 minutes each. Then, the substrates were rinsed by reverse osmosis (RO) water. The substrates were put in the oven at 180 $^{\circ}\text{C}$ for 5 minutes to dry. Next, the substrates were treated in the oxygen plasma at 100 W, for 5 minutes. The SU8 resist was spun at 3000 rpm for 30 sec, and then soft baked for 2 minutes at 95 $^{\circ}\text{C}$ to evaporate the coating solvent and firm down the resist on the top of the SiO_2 after coating. The substrates were cooled down under room temperature before can be patterned. After electron beam patterning, substrates were pre-exposure baked (PEB) for 1 minute at 65 $^{\circ}\text{C}$ and 1 minute at 95 $^{\circ}\text{C}$ and usually SU8 pattern should be visible on the resist surface after PEB process. The SU8 pattern were developed with EC solvent (Ethyl 2-hydroxypropanoate) for 2 minutes, followed by 1 minute of Isopropyl Alcohol (IPA) and dried with nitrogen gun. As a final step, hard-baked was performed at 180 $^{\circ}\text{C}$ on the hotplate for 5 minutes. The fabricated Bragg grating patterns were shown in Figure 1. The fabricated substrates were cleaved and aligned for further experiments.

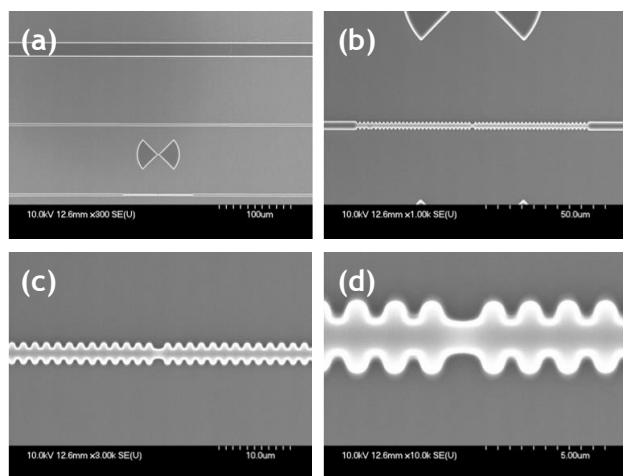


Figure 1 SEM images show the fabricated structure of SU8 polymer waveguide; (a) Reference straight waveguide, 10 μm (top), reference straight waveguide 2 μm (middle) and Bragg grating waveguide 2 μm (bottom)(x0.3k magnification), (b) Bragg grating waveguide (x1.0k magnification), (c) x3.0k magnification, and (d) x10.0k magnification

3.0 EXPERIMENTAL SETUP

The experimental setup consists, depicted in Figure 2 mainly of two parts; controlling the optical component and manipulating the liquid samples. As described earlier, the fabricated devices were characterized by using visible wavelength spectrum under end-facet technique. First part, an optic lamp (100W, 12V, Osram) was used as the main visible light source. HeNe laser (Melles Griot, 5mW) was collimated into the input waveguide and then used as a guiding source during the alignment procedure. After the alignment step, coupling fiber from HeNe laser was shifted to visible light, and visible source will be used as a major source for detection. Translation stage was employed in order to align the light guiding inside the waveguide for both input and output waveguides. Spectral output from the opposite side of input waveguide was collimated into 20X objective lens that was projected onto the fiber optics collector. Then, the output signal was propagated onto the spectrum analyzer (500M, Jobin Yvon Horiba) and captured by charged-coupled device (CCD) (Andor, DU420-BR-DD) camera. Next, the optical responses were scanned and recorded for further analysis. Meanwhile, microfluidic channel system was constructed in order to inject the liquid sample into the sensor surface. Then, the flow of liquid was controlled by programmable syringe pump (World Precision Instrument, AL-1000). Finally, liquid was injected through the microfluidic channels covering the sensing area and then streamed into the waste bottle (Eppendorf® tube).

4.0 RESULTS AND DISCUSSIONS

4.1 Finite-Difference Time-Domain (FDTD) Simulation

The commercially available 2-D FDTD RSoft optical design and analysis software was utilized to simulate the spectrum response characteristics. The structure of polymer Bragg grating waveguide was modelled. The Gaussian pulse was centered at vacuum wavelength of 660 nm was launched into the designated input port. The spectral responses (transmission) of the Bragg grating device were obtained from output port. The device refractive index was set at 1.57 to mimic the polymer material and surrounding area was set up at 1.33 to represent water. We assumed that, when specific biological binding occurred on top of the immobilized protein, more bioanalytes deposited and covered the sensing surface area. This phenomenon will then increased the refractive index of surrounding area. In simulation, we numerically increased the refractive index of surrounding area to imitate the biomolecular binding interaction on the sensing area. According to the Bragg grating model, the change of effective index of the cladding (in our case it was polymer surface), will directly shifted the Bragg wavelength. From this hypothesis, we simulated and recorded the spectral output from the output

waveguide. Figure 2 shows the normalized intensity (a.u) of transmission spectral of polymer Bragg grating device within the visible wavelength region. The simulated device structure parameters consist of waveguide width at 2 μm , grating period at $\Lambda = 323 \text{ nm}$ and grating length of 30 μm . By increasing the refractive index of surrounding medium from 1.33 to 1.34, the transmission spectrum was shifted to the right of the spectrum region as depicted in Figure 3. Then we gradually increased the refractive index until 1.43. From the simulation, the spectral shift stretches approximately to 53.7 nm due to the increase of 0.1 refractive index of surrounding sensing area.

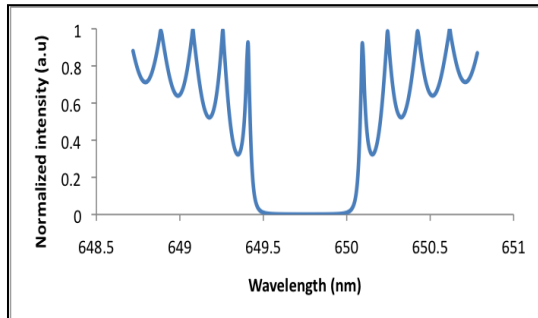


Figure 2 Simulated spectral response (transmission spectra) of polymer Bragg grating device within the visible wavelength region

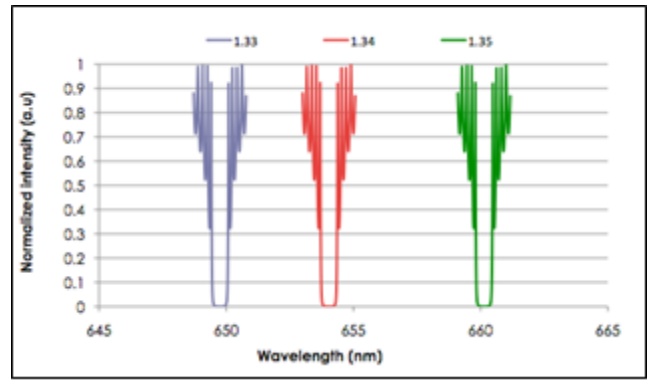


Figure 3 Spectral shift (blue dashed arrow) due to the refractive index changes of surrounding sensing medium. The spectral shift (from left to right) occurred at different refractive index respectively

4.2 Experimental

In order to demonstrate the applicability of the device in biosensing, a measurement was carried out to characterize the fabricated Bragg grating waveguide with the dimension of 2 x 2 μm (width x height). Figure 5 shows the normalized intensity (a.u) of spectral shift response of polymer Bragg grating waveguide within the visible wavelength region. In order to clarify the measurement of the resonance shift, the recorded spectra in Figure 4 was simplified as in Figure 5, where the x-axis was expanded and resonance peak was traced to make it easier to see the shift in resonance peak. Since the base solution for this experiment was the DI water, the initial resonance response at $t = 0 \text{ s}$ was recorded when the sensor area was filled with the DI water. A reference spectral drop was measured at $\lambda = 668.587 \text{ nm}$. The concentrations of the mixed sucrose solution corresponding to these measurements were derived from Table 1.

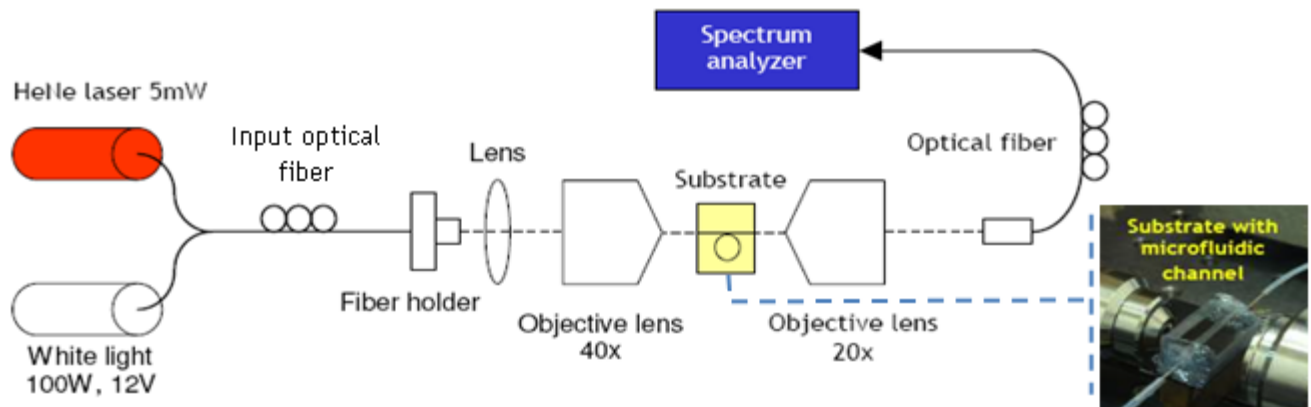


Figure 4 Schematic diagram of the measurement setup used for device characterization and experiments. The HeNe laser is used for input and output coupling alignment; the substrate is manipulated using a 3-axis stage to achieve the highest reading. When the maximum intensity is obtained from the spectrum analyzers, the input optical fiber is switched to the white light source

By monitoring the chosen drop in Figure 5, it was clearly seen that the selected spectrum was displaced from the value in DI water of $\lambda = 668.587$ nm to a higher wavelength of $\lambda = 671.112$ nm when we mixed 10% of sucrose solution into the sensing channel. Then, the chosen drop was steadily increased to $\lambda = 672.505$ nm and $\lambda = 673.723$ nm with mixing solution of sucrose at 20 % and 30% respectively. As we mentioned earlier,

the mixed solutions from the outlet of microfluidic channel were collected in Eppendorf® tubes and the refractive indices of these mixing solution were measured by using Abbe Refractometer. The full experimental results of spectral shift against the increasing sucrose concentration is plotted and shown in Figure 5.

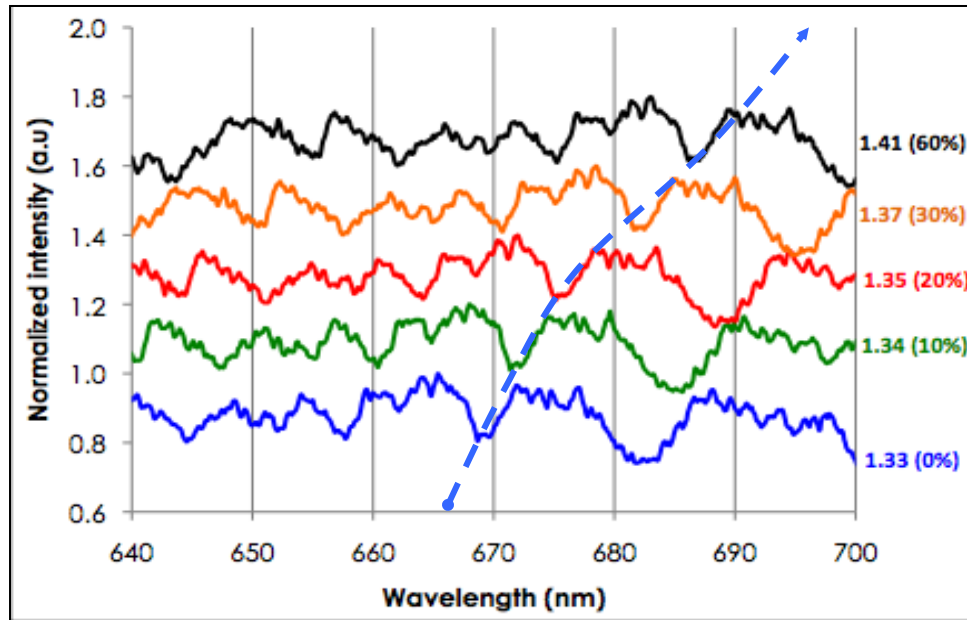


Figure 5 Normalized intensity of resonance wavelength pattern at different mixing stage period (%) of experiment. The wavelength region was projected between $\lambda = 630 - 700$ nm and the plotted lines were vertically displaced for the ease of comparison. The (blue dashed arrow) shows the tracked of spectral drop position upon the time duration and mixing stage percentage

Table 1 The result of sucrose concentration solution, refractive index measurement and spectral shift (nm) from experiment and simulation

Sucrose solution (%)	Refractive index*	Spectral shift, nm (Simulation)	Spectral shift, nm (Experiment)
0 %	1.3333	0	0
10 %	1.3461	4.984	2.525
20 %	1.3618	11.021	6.268
30 %	1.3781	22.935	10.272
60 %	1.4310	53.738	20.379

* Abbe refractive index

From this, it appeared that the spectral shifts for the pre-made 10, 20 and 30% solutions make an over estimate of the sucrose concentration. For comparison between simulation and experimental works, graph was plotted as in Figure 6. According to

Figure 6, spectral shift responses for both FDTD simulation and experiment show a linear relationship between spectral shifts upon sucrose refractive index. However, we only obtained half value of the spectral shift from the experiment compared to FDTD simulation at certain refractive index unit. We suspected that the discrepancies were likely due to the accumulation of sucrose solution on top and sidewall of the sensing area, causing the interaction of evanescent tail imprecise to actual sucrose concentration as calculated. The insertion loss between input and output coupling of the waveguide interface also reduced the intensity of selected spectral wavelength during the experiments, where it was can't be performed in simulation. Another possible factor that affect the experimental output value was the temperature drift within the sensing area and polymer Bragg grating respectively, that induced the noise to signal ratio.

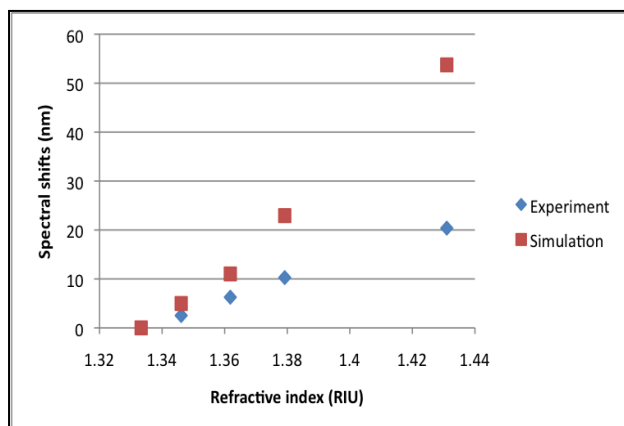


Figure 6 Comparison of spectral shift between simulation and experimental characterization of polymer Bragg grating waveguide at certain refractive index of surrounding sensing area

In order to overcome this circumstances, we are planning to employ a temperature control, such as a thermoelectric cooler (Peltier effect device) to stabilize temperature in future. This procedure hopefully will lead to better precision in the determination of spectral shifts especially in experiment.

As preliminary results, a linear relationship shows between the spectral shifts within the visible wavelength region and the sucrose refractive index value. The sensitivity was still low compared to the Mach-Zehnder or microring resonator system. However, we can see the the ability of Bragg grating structure to sense the RI changes of sensing area without etching process or complex structural design. Due to the large grating pitch, they are also far easier to fabricate and the use of visible wavelength region has the potential to facilitate the measurement that demand a small changes with greater precision, especially in both label and label-free biosensing applications.

5.0 CONCLUSIONS

In this study, we demonstrated the SU8 polymer Bragg grating waveguide as an optical biosensing. The straightforward procedure of SU8 polymer fabrication process has revealed an important role in rapid fabrication steps without performing a number of fabrication stages and layers. We validated the device by simulating the polymer Bragg grating waveguide, performing the experiment upon the polymer fabricated device and monitoring the output spectral response in real time. Both simulation and experiment were based on variation of refractive index of sucrose concentration solution. It was demonstrated that the fabricated polymer Bragg grating waveguide could be used to measure the refractive index of a sucrose solution (bulk

detection). When the refractive index of the surrounding sensing area was changed (because of sucrose solution), the Bragg spectral was also shifted by approximately 530 nm/RIU (simulation) and 200 nm/RIU (experiment). Future work will include the system to monitor changes in the refractive index of surrounding media and binding of specific proteins.

Acknowledgment

The authors would like to thank Bioelectronics Group and James Watt Nanofabrication Centre (JWNC) staff and technicians, Glasgow University. We also like to acknowledge for fully funded RACE Grant from Ministry of Higher Education Malaysia (MOHE), International Islamic University Malaysia (IIUM) and also partly funded by Intillogic Enterprise.

References

- [1] Cooper, M.A. 2009. *Label-Free Biosensor: Techniques and Applications*. Cambridge University Press, UK.
- [2] H. K. Hunt and A. M. Armani. 2010. Label-free Biological And Chemical Sensors. *Nanoscale*. 2: 1544-1559.
- [3] S. P. Wang, A. Ramachandran, and S. J. Ja. 2009. Integrated Microring Resonator Biosensors for Monitoring Cell Growth and Detection of Toxic Chemicals in Water. *Biosensors & Bioelectronics*. 24: 3061-3066.
- [4] B. E. Little, S. T. Chu, H. A. Haus, J. Foresi, and J. P. Laine. 1997. Microring Resonator Channel Dropping Filters. *Journal of Lightwave Technology*. 15: 998-1005.
- [5] D. Lee, T. Lee, J. Park, S. Kim, W. Hwang, and Y. Chung. 2007. Widely Tunable Double-Ring-Resonator Add/Drop Filter Using High-Index-Contrast Polymer Waveguide. 1(4): 822-8231441.
- [6] A. Ramachandran, S. Wang, J. Clarke, S. J. Ja, D. Goad, L. Wald, E. M. Flood, E. Knobbe, J. V. Hryniewicz, S. T. Chu, D. Gill, W. Chen, O. King, and B. E. Little. 2000. A Universal Biosensing Platform Based on Optical Micro-Ring Resonators. *Biosensors & Bioelectronics*. 23: 939-944.
- [6] L. Caruso and I. Montrosset. 2003. Analysis of a Racetrack Microring Resonator with MMI Coupler. *Journal of Lightwave Technology*. 21: 206-210.
- [7] A. Yariv. 2002. Critical Coupling and Its Control in Optical Waveguide-Ring Resonator Systems. *IEEE Photonics Technology Letters*. 14: 483-485.
- [8] F. Vollmer, D. Braun, A. Libchaber, M. Khoshshima, I. Teraoka, and S. Arnold. 2002. Protein Detection by Optical Shift of a Resonant Microcavity. *Applied Physics Letters*. 80: 4057-4059.
- [9] N. M. Hanumegowda, I. M. White, H. Oveys, and X. D. Fan. 2005. Label-free Protease Sensors Based on Optical Microsphere Resonators. *Sensor Letters*. 3: 315-319.
- [10] J. P. Guo, M. J. Shaw, G. A. Vawter, G. R. Hadley, P. Esherick, and C. T. Sullivan. 2005. High-Q Microring Resonator for Biochemical Sensors. *Integrated Optics: Devices, Materials, and Technologies IX*. 5728: 83-92368.
- [11] A. Yalcin, K. C. Popat, J. C. Aldridge, T. A. Desai, J. Hryniewicz, N. Chbouki, B. E. Little, O. King, V. Van, S. Chu, D. Gill, M. Anthes-Washburn, and M. S. Unlu. 2006. Optical Sensing of Biomolecules Using Microring Resonators. *IEEE Journal of Selected Topics in Quantum Electronics*. 12: 148-155.
- [13] D. X. Xu, M. Vachon, A. Densmore, R. Ma, A. Delage, S. Janz, J. Lapointe, Y. Li, G. Lopinski, D. Zhang, Q. Y. Liu, P. Cheben, and J. H. Schmid. Label-free Biosensor Array

- based on silicon-on-insulator Ring Resonators Addressed Using a WDM Approach. *Optics Letters*. 35: 2771-2773.
- [14] R. W. Boyd and J. E. Heebner. 2001. Sensitive Disk Resonator Photonic Biosensor. *Applied Optics*. 40: 5742-5747.
- [15] Y. Z. Sun, S. I. Shopova, G. Frye-Mason, and X. D. Fan. 2008. Rapid Chemical-Vapor Sensing Using Optofluidic Ring Resonators. *Optics Letters*. 33: 788-790.
- [16] S. Arnold, R. Ramjith, D. Keng, V. Kolchenko, and I. Teraoka. 2008. MicroParticle Photophysics Illuminates Viral Bio-Sensing. *Faraday Discussions*. 137: 65-83.
- [17] A. M. Armani and K. J. Vahala. 2006. Chemical and Biological Detectors Using Ultra-High-Q Microresonators. *Optomechatronic Micro/Nano Devices and Components II*. 6376: U48-U57215.
- [18] H. K. Hunt, C. Soteropulos, and A. M. Armani. 2010. Bioconjugation Strategies for Microtoroidal Optical Resonators. *Sensors*. 10: 9317-9336.
- [19] A. Densmore, D. X. Xu, P. Waldron, S. Janz, T. Mischki, G. Lopinski, J. Lapointe, A. Delage, E. Post, C. Storey, P. Cheben, B. Lamontagne, and J. H. Schmid. 2008. Densely Folded Silicon Photonic Wire Biosensors in Ring Resonator and Mach-Zehnder Configurations. *Conference on Lasers and Electro-Optics & Quantum Electronics and Laser Science Conference*. 1-9: 1947-19483638.
- [20] F. Vollmer and S. Arnold. 2008. Whispering-gallery-mode Biosensing: Label-Free Detection Down to Single Molecules. *Nature Methods*. 5: 591-596.
- [21] V. M. N. Passaro, F. Dell'Olio, B. Casamassima, and F. De Leonardis. Guided-wave Optical Biosensors. *Sensors*. 7: 508-536.
- [22] K. De Vos, J. Girones, S. Popelka, E. Schacht, R. Baets, and P. Bienstman. 2009. SOI Optical Microring Resonator with poly(ethylene glycol) Polymer Brush For Label-free Biosensor Applications. *Biosensors & Bioelectronics*. 24: 2528-2533.
- [23] C. A. Barrios, B. Sanchez, K. B. Gylfason, A. Griol, H. Sohlstrom, M. Holgado, and R. Casquel. 2007. Demonstration of Slot-Waveguide Structures on Silicon Nitride/Silicon Oxide Platform. *Optics Express*. 15: 6846-6856.
- [24] D. X. Dai, B. Yang, L. Yang, Z. Sheng, and S. L. He. 2009. Compact Microracetrack Resonator Devices Based on Small SU-8 Polymer Strip Waveguides. *IEEE Photonics Technology Letters*. 21: 254-256.
- [25] G. T. Palocz, Y. Y. Huang, A. Yariv, and S. Mookherjee. 2003. Polymeric Mach-Zehnder Interferometer Using Serially Coupled Microring Resonators. *Optics Express*. 11: 2666-2671.
- [26] B. H. Ong, X. Yuan, S. Tao, and S. C. Tjin. 2006. Photothermally Enabled Lithography for Refractive-Index Modulation in SU-8 Photoresist. *Optics Letters*. 31: 1367-1369.
- [27] B. Y. Shew, C. H. Kuo, Y. C. Huang, and Y. H. Tsai. 2005. UV-LIGA Interferometer Biosensor Based on the SU-8 Optical Waveguide. *Sensors and Actuators a-Physical*. 120: 383-389.
- [28] M. H. M. Salleh, A. Glidle, J.M Cooper. 2010. Characterization of SU8 Polymer Gapless Disk Resonators Using Visible Wavelength Light Source. *Optics and Photonics 2010 (Photon10)*. University of Southampton, U.K, 23rd– 26th August 2010.
- [29] E. S. Hosseini, S. Yegnanarayanan, A. H. Atabaki, M. Soltani, and A. Adibi. 2009. High Quality Planar Silicon Nitride Microdisk Resonators for Integrated Photonics in the Visible Wavelength Range. *Optics Express*. 17: 14543-14551.